Electronic Supplementary Information

Enhancing Functionalities of Organic Ultraviolet–Visible Phototransistors Incorporating Spiropyran–Merocyanine Photochromic Materials

*Ren – Jie Wu, Yueh – Ling Hsu, Wei – Yang Chou and Horng – Long Cheng**

Department of Photonics, Advanced Optoelectronic Technology Center, National Cheng Kung University, Tainan 701, Taiwan

*Corresponding Author: Horng–Long Cheng (Email: shlcheng@mail.ncku.edu.tw)

Outline

1. Supplementary IR and XPS spectra of the PVP:SP–MC blend films

Methods: The IR spectrum was recorded with a FT–IR spectrometer (Vertex 70, Bruker) using the attenuated total reflection method for sample preparation technique with a range of 1000–4000 cm^{-1}. The theoretical calculations of the molecular IR spectra and their vibrational modes were performed using DFT at B3LYP/6–31(d) level of theory. X-ray photoelectron spectroscopy (XPS) analysis was performed with a multi-purpose XPS (Sigma Probe, Thermo VG-Scientific) by using a monochromatic Al Kα radiation X-ray source (12 kV, KE = 1486.6 eV).

Analysis and Discussion: After UV light irradiation, many SP molecules were converted into MC form in the PMMA:SP blend film, which can be confirmed by absorption spectroscopy (Fig. 2a). The corresponding IR spectrum is shown in trace b of Fig. S1. By comparing the experimental and computed IR spectra, the MC form does exist in the UV–irradiated PMMA matrix film because its most important characteristic peaks can be observed and conform to the theoretical prediction, such as C=O bond stretching (1650 cm^{-1}), C=C (vinyl) stretching (1500–1600 cm^{-1}), N–O stretching (1330–1350 cm^{-1}) and N–C stretching (1075 cm^{-1}) vibrational modes. These peaks (such as C–O–C stretching and C=O stretch of ester)[s1,s2] from the PMMA matrix (trace a of Fig. S1) can also be seen.

Despite the background signal of PVP matrix (trace d of Fig. S1, e.g., C=C ring stretching [1500–1600 cm^{-1}], C–O bending [1400–1500 cm^{-1}] and O–H in–plane bending mode of phenol group [1170 cm^{-1}]),[s1–s5] these important characteristic peaks of the MC form can also be seen in the PVP:SP–MC blend films without UV light irradiation (trace c of Fig. S1), confirming the existence of the MC form. The formation of hydrogen bonding between the MC molecules and PVP in the films can also be studied by IR spectroscopy. IR spectroscopy has been used to predict the formation of hydrogen bonds between the hydroxyl groups in PVP and the carbonyl and hydroxyl groups of other molecules.[s1–s5] PVP has a peak centred at 3540 cm^{-1}, which is attributed to free hydroxyl groups (nonbonded OH), and a broad band at approximately 3100–3500 cm^{-1}, which represents a broad distribution of self–associated hydroxyl groups (hydrogen–bonded OH). The relative intensity of the 3540 cm^{-1} band has been reported to decrease with the increasing intensity of hydrogen bonding and is barely detected in the spectra of blends with strong hydrogen bonds, whereas a high–frequency shift of the broad hydrogen–bonded hydroxyl band is observed.[s1–s5] Their IR data also reveal reduced intensity of the H–bonded OH vibrations relative to that of the C–H stretching vibrations.[s1,s2,s5] Fig. S1 reveals a broad band centred at 3340 cm^{-1} of the PVP:SP–MC blend film, indicating the formation of hydrogen bonding. Compared with the IR spectra of pure PVP film (trace d) and that reported in the literature,[s1–s5] the following observations may reflect the existence of hydrogen bonds between MC and PVP, such as this unclear 3540 cm^{-1} peak (free OH vibrations), and slight blue shift and reduced intensity (relative to C–H vibrations) of the H–bonded OH vibrations.

The carbonyl stretching region in the IR spectroscopy can also be used to study the hydrogen bonds due to the formation of hydrogen bonding causing the carbonyl stretching band to shift to a lower wavenumber. [s1–s4] Although the signal of the carbonyl stretching band of the MC molecule

in the PVP and PMMA matrix films is not strong, it may still provide useful information about the hydrogen bonds. The carbonyl stretching region (1630–1670 cm^{-1}) displayed in the inset of Fig. S1 reveals that the spectrum of the PVP:SP–MC blend film is dominated by a band centred at 1648 cm^{-1} assigned to hydrogen–bonded carbonyl groups, but a shoulder is observed at longer wavenumbers near 1656 cm^{-1} assigned to free carbonyl groups (nonhydrogen–bonded). By contrast, the C=O stretching mode of the MC molecule in the UV–irradiated PMMA:SP blend film is dominated by a band at 1656 cm^{-1}. Moreover, no remarkable shift of the C=O stretching band of the PMMA in the UV–irradiated PMMA:SP blend film is observed compared with a band associated with the OH···O=C interaction at lower wavenumbers near 1706 cm^{-1}.[s1–s2] Furthermore, no clear signal of hydrogen–bonded OH band is observed in the range of 3200–3600 cm^{-1} of the UV–irradiated PMMA:SP blend film. Thus, we conclude that the MC form in the PMMA matrix corresponds to no evident hydrogen bond case.

In addition to the formation of hydroxyl–carbonyl hydrogen bonds, the hydrogen bonds between the hydroxyl group of PVP and the nitro group of the MC can be formed. Compared with UV–irradiated PMMA:SP blend film, only slight spectral shifts of the N–O bond peaks (1320–1370 cm^{-1}) in the PVP:SP–MC blend film are observed (inset of Fig. S1). Hydrogen bonding can also cause a shift of the $-NO_2$ band due to different degrees of resonance on H–bonding and the change in planarity of the NO_2 group with the ring.[s6] Owing to the weakly basic character of the nitro group, spectral shifts of OH proton donors bonding to nitro compounds are expected to be small.[s7] Moreover, the N–O band broadening of the MC in the PVP matrix compared with that in the PMMA matrix is likely due to hydrogen bonding.[s6,s8]

Fig. S2a shows the O 1s core-level spectra of pure PVP and PVP:SP–MC blend films. The O 1s electrons of the pure PVP film has a binding energy (BE) of 534.4 eV. The O 1s peak of the pure PVP film can be deconvoluted into two component peaks, i.e. 534.4 and around 533.3 eV. The presence of low-BE component is attributed to the oxygen involved in the formation of hydrogen bonds between hydroxyl groups.[s9,s10] In the PVP:SP–MC blend film, the peak broadening of high-BE components reflects the possible contribution from oxygen in SP/MC molecules. The O 1s BEs in NO_2 and C–O–C are reported at around 533[s11] and 534[s12] eV, respectively. However, the carbonyl group in MC dyes shows low O 1s BE ranging from 530.6 eV to 531.6 eV.[s12] These O 1s signals of SP/MC molecules overlap with the O 1s signals of PVP, making the analysis difficult. However, the low-BE O 1s peak in the PVP:SP–MC blend film significantly shifts to low BE, which may reflect the formation of hydrogen bonding between PVP and MC.

Fig. S2b shows the comparison of N 1s core-level spectra between the PMMA:SP and PVP:SP–MC blend films. SP molecules exist in the PMMA film without UV light irradiation. The N 1s spectrum of the PMMA:SP blend film can be resolved into two component peaks, i.e. nitro group at 405.8 eV and heterocyclic N at 399.4 eV of the SP molecule.[s13,s14] In the PVP:SP–MC blend film, the heterocyclic N 1s peak shifts significantly to higher energy at 400.8 eV, indicating the existence of the MC form.[s13] In addition, the nitro N 1s BE increases by 1.0 eV, and the large shift suggests the formation of a strong hydrogen bond.[s15] Such a decrease in the O 1s BE and an

increase in the N1s BE are also observed between the hydroxyl and pyridyl groups due to the formation of hydrogen bonding.[s15]

In accordance with the results of absorption, IR and XPS spectra, Fig. S3 shows the potential hydrogen bonding interactions that can be involved in the MC and PVP system.

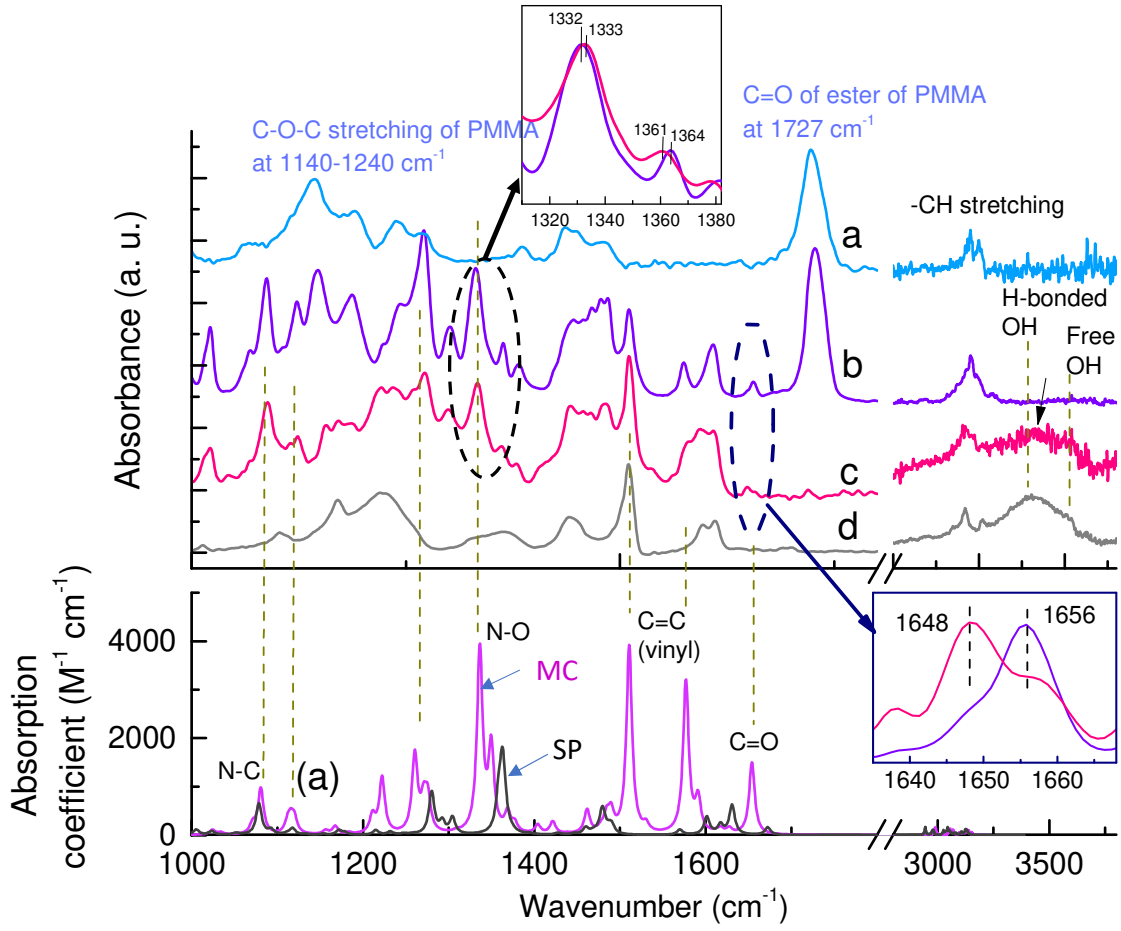

Fig. S1 Upper panel: Experimental IR spectra of (a) PMMA, (b) UV–irradiated PMMA:SP (3:5) blend, (c) PVP:SP–MC (3:5) blend, and (d) PVP films. Lower panel: Theoretical calculated IR spectra (scaling factor of 0.963) of MC (purple) and SP (black) molecules. Inset: Enlarged IR spectra of UV–irradiated PMMA:SP (3:5) blend (blue violet) and PVP:SP–MC (3:5) blend (red) films in the range of 1630–1670 cm^{-1} and 1310–1380 cm^{-1}.

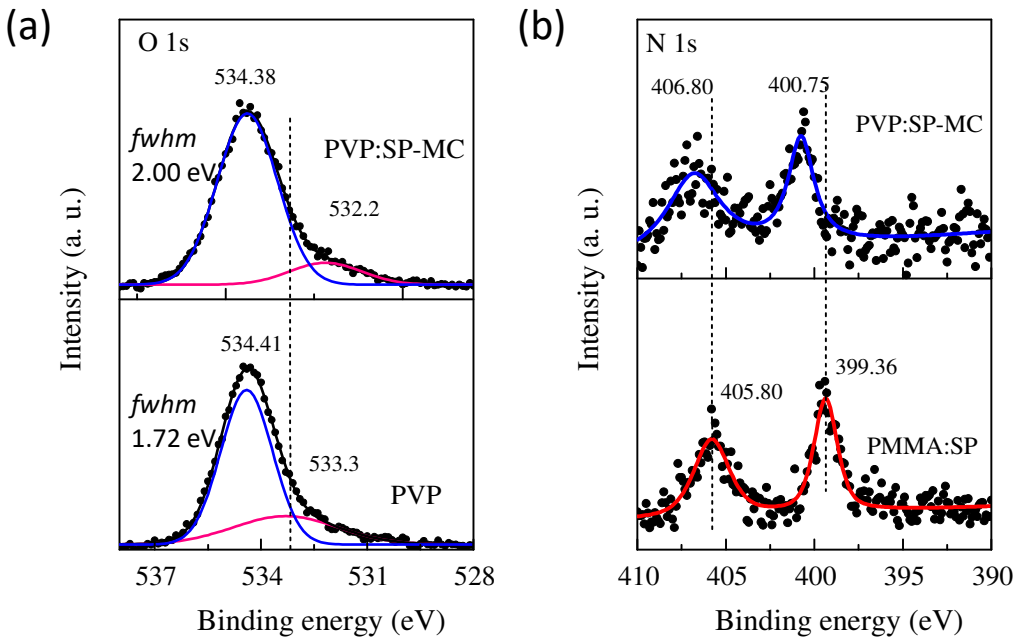

Fig. S2 (a) O 1s XPS spectra of pure PVP and PVP:SP–MC blend films. The full width at half-maximum (*fwhm*) of the O 1s peak at around 534.4 ev is shown. (b) N 1s XPS spectra of the PMMA:SP and PVP:SP–MC blend films. The Gaussian/Lorentzian functions used for the deconvolution are presented by a thin solid line. The thick solid lines represent the oval fit, while the dots to the experimental data. The vertical dashed lines are guide for the eye.

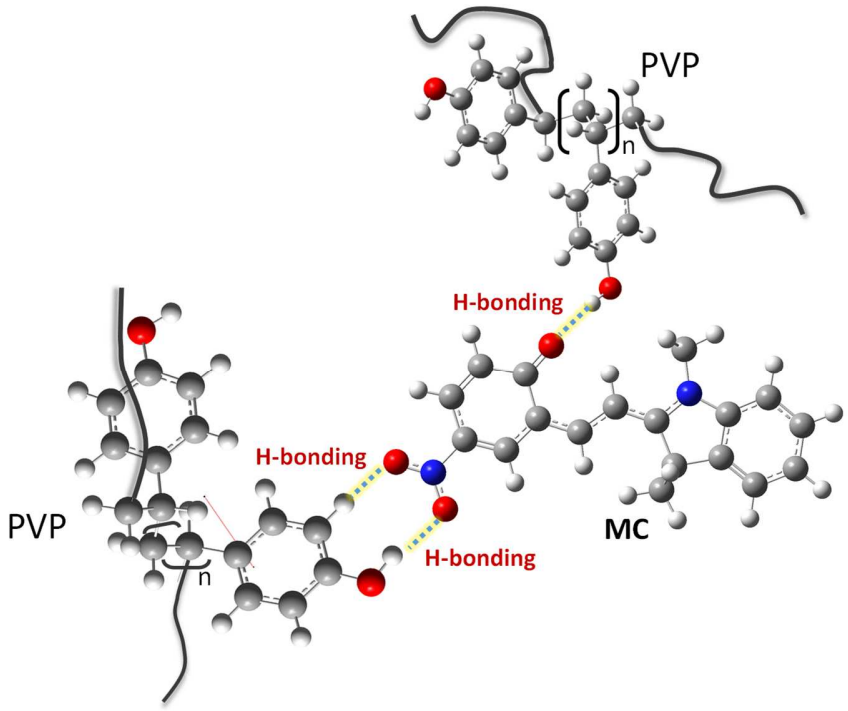

Fig. S3 Potential hydrogen–bonding involved in the PVP–MC system.

2. Supplementary data for the stability of MC in the PVP matrix

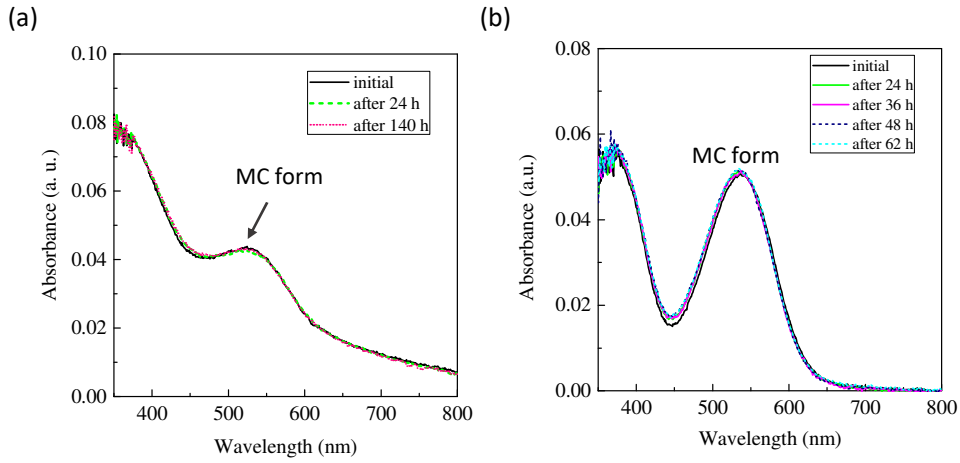

Fig. S4 Absorption spectra measured at different times: (a) PVP:SP blend (3:5 *w/w* in preparation) in n–butanol solution; (b) PVP:SP blend (1:1 *w/w* in preparation) solid film. The arrow indicates the presence of a small amount of the MC form in the solution.

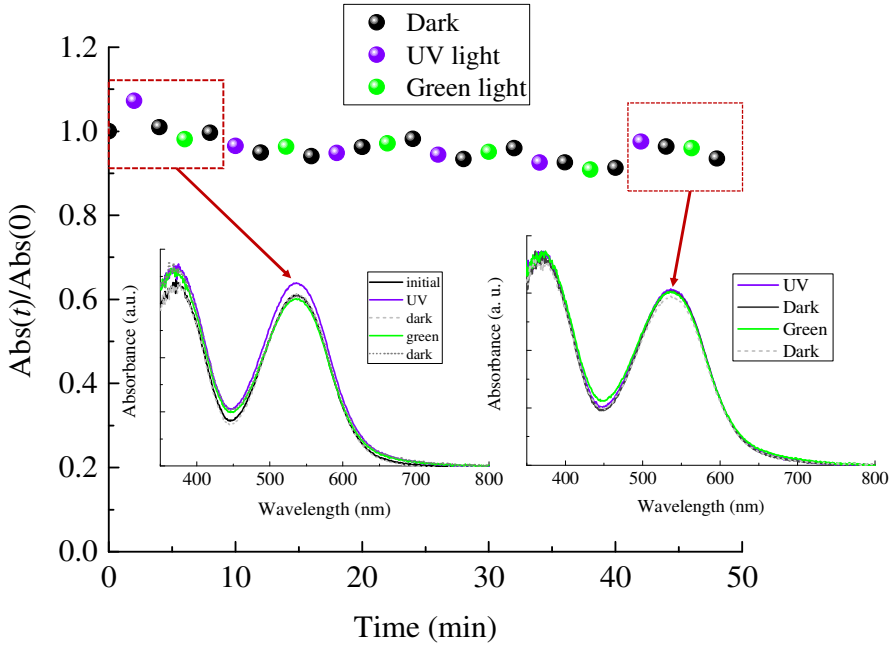

Fig. S5 Normalised absorbance at 530 nm as a function of time of the PVP:SP–MC (3:5) blend film before and after repeating the following procedure several times in succession: Irradiate UV light (55 μW/cm^2), place in the dark, irradiate green light (1 mW/cm^2), and then in the dark for 2 min each. Abs(0) and Abs(t) are the absorbance at the initial and at a given time, respectively. Here, the time to measure the spectrum is ignored. The selected absorption spectra at the given time are shown in the inset.

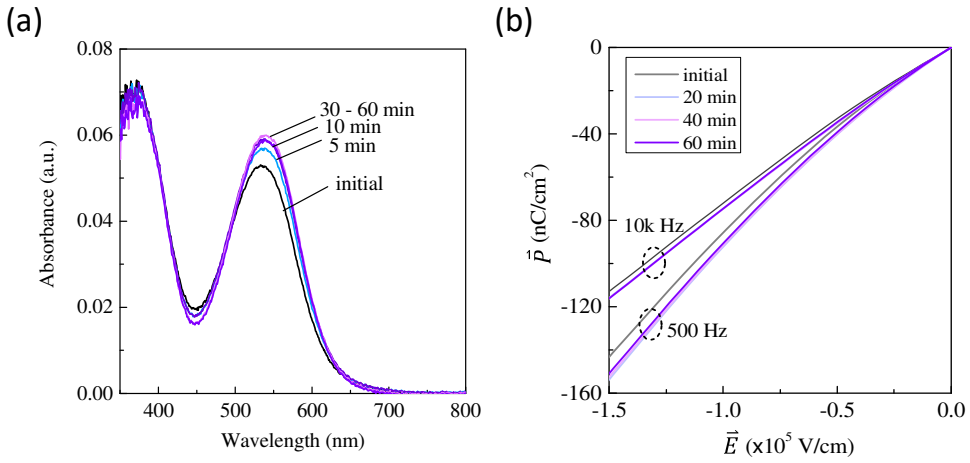

Fig. S6 (a) Absorption spectra of the PVP:SP–MC (3:5) blend films and (b) $\vec{P}-\vec{E}$ curves of the PVP:SP–MC (3:5) blend–based (3:5) MISM devices before and after continuous UV irradiation (55 μW/cm^2) for a period of time. The increase in absorbance at 530 nm and the slope χ_e of $\vec{P}-\vec{E}$ curves caused by the UV irradiation may reflect the conversion of residual SP molecules into the MC form. After 60 min of continuous exposure to UV light, these results indicate that the as–prepared PVP:SP–MC blend films are quite stable.

3. Gap–tunning procedure

Reliable descriptions of ionization potential (IP), electron affinity (EA) and optical gap (E_{opt}) were obtained according to electronics properties calculated through DFT/TDDFT with the LRC functional CAM–B3LYP and 6–311G+(d,p) basis set based on optimized geometrics. The range separation parameter ω of the LRC functional was optimized by minimizing the expression $J(\omega)$, that is, the so–called gap–tuning procedure was performed.[s16]

$$J(\omega) = J_{IP}(\omega) + J_{EA}(\omega) \quad \text{(s1)}$$

$$J_{IP}(\omega) = |E_+(\omega) - E_0(\omega) + \epsilon_0^H(\omega)| \quad \text{(s2)}$$

$$J_{EA}(\omega) = |E_0(\omega) - E_-(\omega) + \epsilon_-^H(\omega)| \quad \text{(s3)}$$

where $\epsilon_0^H(\omega)$ and $\epsilon_-^H(\omega)$ are the levels of HOMO energy in the neutral and anionic states of a molecule, respectively, and $E_0(\omega)$, $E_+(\omega)$ and $E_-(\omega)$ are the total energy levels of the neutral, cationic and anionic states, respectively. The impact of surrounding dielectric medium was considered by incorporating the polarizable continuum medium (PCM) characterized by a dielectric constant into the DFT/TDDFT calculations. The ω value of the LRC functional was optimized and tuned in the presence of dielectrics.

Table S1 Gap–tunning procedure for the SP, MC, and pentacene molecules at different dielectric environments: calculated ionization potential (IP), electron affinity (EA) and $J(\omega)$ at various range separation parameter ω conditions.

Species	ε_r	ω (bohr^{-1})	IP (eV)	EA (eV)	$J(\omega)$	ε_r	ω (bohr^{-1})	IP (eV)	EA (eV)	$J(\omega)$
SP	4	0.5	6.046	1.849	0.0754	13.4	0.1	5.508	1.991	0.0337
		0.1	5.807	1.599	0.0109		0.05	5.478	1.978	0.0126
		0.05	5.781	1.590	0.0100		0.04	5.475	1.977	0.0079
		0.03	5.775	1.588	0.0196		0.03	5.474	1.976	0.0060
		0.01	5.773	1.589	0.0297		0.01	5.470	1.977	0.0072
		0.005	5.774	1.590	0.0323		0.005	5.471	1.978	0.0098
MC	4	0.07	5.580	2.413	0.0151	13.4	0.05	5.334	2.675	0.0264
		0.05	5.571	2.407	0.0069		0.01	5.323	2.670	0.0073
		0.03	5.564	2.403	0.0022		0.005	5.323	2.670	0.0047
		0.01	5.560	2.402	0.0122		0.001	5.323	2.671	0.0027
		0.005	5.560	2.403	0.0147		0.0005	5.323	2.671	0.0024
		0.001	5.560	2.403	0.0168		0.0001	5.323	2.671	0.0027
Pentacene	4	0.5	5.055	2.247	0.0611	13.4	0.1	4.628	2.443	0.0431
		0.1	4.850	2.142	0.0239		0.05	4.581	2.442	0.0257
		0.05	4.804	2.142	0.0066		0.01	4.567	2.441	0.0069
		0.01	4.790	2.142	0.0123		0.005	4.567	2.442	0.0043
		0.005	4.790	2.143	0.0148		0.001	4.567	2.442	0.0022
		0.001	4.791	2.143	0.0169		0.0005	4.567	2.442	0.0020

4. Crystalline properties of the pentacene films

Table S2 The crystallographic parameters calculated from the XRD data of pentacene films deposited on the neat PVP film and the PVP:SP–MC blend films, including d_{001}–spacing, average crystalline sizes, and degrees of structural disorder.

Sample	Thin–film phase d_{001}–spacing[a] (nm)	Bulk phase d_{001}–spacing[a] (nm)	Average crystalline size[b] (nm)	Structural disorder[b] (%)
PVP	1.53	–	31.62	1.53
PVP:SP = 5:3	1.53	–	31.62	1.42
PVP:SP= 1:1	1.53	1.43	31.62	1.81
PVP:SP = 3:5	1.53	1.44	31.81	1.76

[a] The values of d_{001}–spacing of thin–film phase and bulk phase were extracted from XRD data according to our published papers.[s17,s18]

[b] Average crystalline size and structural disorder of thin–film phase were obtained based on paracrystal theory, following our previous methodology.[s17]

5. *C–V* measurement data of the pentacene–based MSIM devices

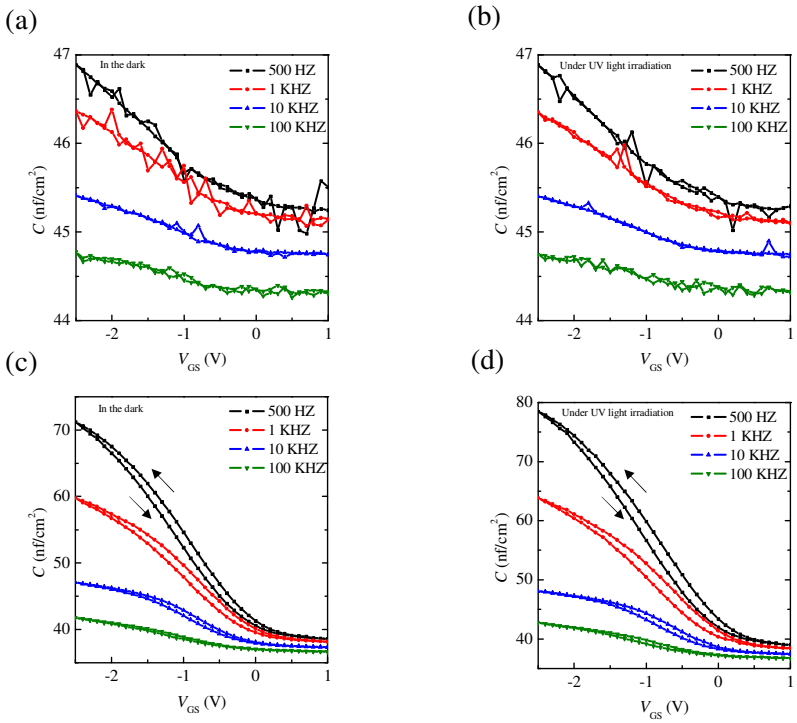

Fig. S7 *C–V* curves of (a, b) neat PVP–based and (c, d) PVP:SP–MC (3:5) blend–based MISM devices under dark condition and UV light irradiation.

6. Schematic diagrams of optimized molecular structures and dipole moments

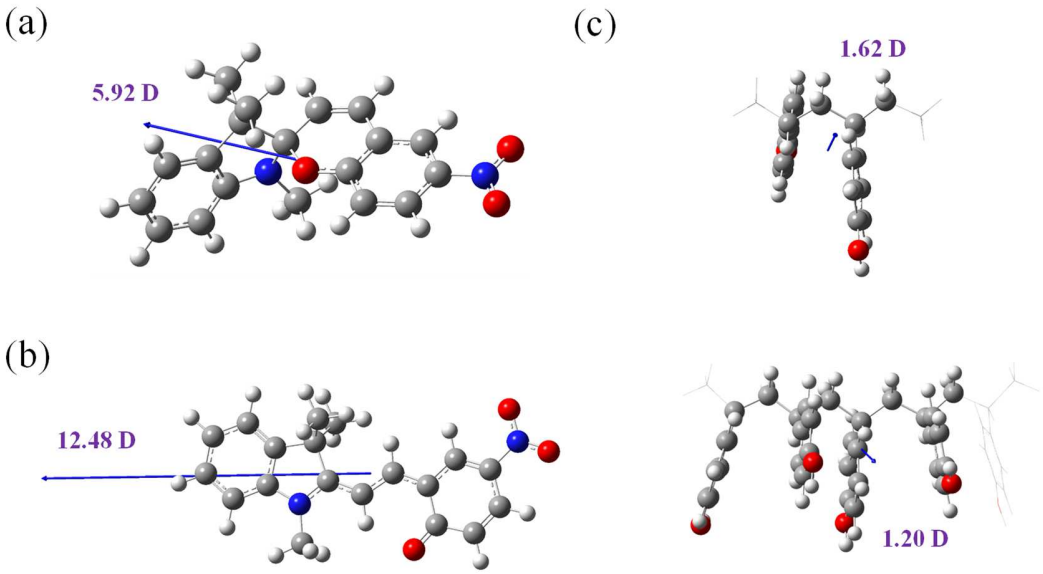

Fig. S8 Optimized molecule structures of (a) SP, (b) MC, and (c) PVP with two and five repeat units. The calculated magnitude and direction of dipole moment are shown. For PVP calculation,

2–layer ONIOM method (i.e., Our own N–layered Integrated molecular Orbital and molecular Mechanics)[s19] was applied. Higher layer (presented as ball–and–bond type) and lower layer (presented as wireframe type) were optimized at B3LYP/6–311G+(d,p) and B3LYP/3–21G*, respectively.

7. Electron excitation analysis of the SP and MC molecules

Table S3 Excitation energy (E_{opt}), t index, D index, S_r index and $\Delta\mu_D$ for a SP molecule in the gas phase and the solid state with various dielectric constants. Only these states with energy less than 3.4 eV are shown.

E_{opt} (eV)	Excitation type	t (Å)	D (Å)	S_r (a.u.)	$\Delta\mu_D$ (D)
In gas phase					
2.78	LE ($S_0 \rightarrow T_1$)	-1.10	1.04	0.85	4.98
2.96	LE ($S_0 \rightarrow T_2$)	-0.80	0.55	0.78	2.63
3.23	LE ($S_0 \rightarrow T_3$)	-0.10	2.45	0.73	11.78
3.31	LE ($S_0 \rightarrow T_4$)	-0.73	0.63	0.51	3.03
In solid state with dielectric constant of 4.0					
2.65	LE ($S_0 \rightarrow T_1$)	-0.20	2.13	0.75	10.24
2.99	LE ($S_0 \rightarrow T_2$)	-2.11	0.15	0.83	0.70
3.09	LE ($S_0 \rightarrow T_3$)	-1.73	0.91	0.83	4.37
3.34	LE ($S_0 \rightarrow T_4$)	-0.51	0.70	0.50	3.34
In solid state with dielectric constant of 13.4					
3.04	LE ($S_0 \rightarrow T_1$)	-1.71	0.78	0.83	3.73
3.15	LE ($S_0 \rightarrow T_{2)}$	-1.82	0.20	0.82	0.97

Table S4 Excitation energy (E_{opt}), t index, D index, S_r index and $\Delta\mu_D$ for a MC molecule in the gas phase and the solid state with various dielectric constants. Only these states with energy less than 3.4 eV are shown.

E_{opt} (eV)	Excitation type	t (Å)	D (Å)	S_r (a.u.)	$\Delta\mu_D$ (D)
In gas phase					
1.395	LE ($S_0 \rightarrow T_1$)	-1.43	1.22	0.77	5.87
2.260	CT ($S_0 \rightarrow T_2$)	0.51	1.99	0.39	9.56
2.392	LE ($S_0 \rightarrow T_3$)	-2.21	0.39	0.79	1.85
2.466	CT ($S_0 \rightarrow S_1$)	0.72	2.21	0.40	10.63
2.550	LE ($S_0 \rightarrow S_2$)	-1.28	1.40	0.74	6.73
2.797	CT ($S_0 \rightarrow T_4$)	0.37	2.37	0.64	11.36
2.956	LE ($S_0 \rightarrow T_5$)	-0.77	1.02	0.77	4.89
3.160	LE ($S_0 \rightarrow T_6$)	-0.37	1.63	0.46	7.81
3.341	LE ($S_0 \rightarrow T_7$)	-3.09	0.69	0.89	3.33
3.349	LE ($S_0 \rightarrow S_3$)	-2.65	0.64	0.73	3.07
Dielectric constant = 4					
1.564	LE ($S_0 \rightarrow T_1$)	-1.74	0.86	0.72	4.10
2.374	LE ($S_0 \rightarrow T_2$)	-2.16	0.35	0.82	1.67
2.487	CT ($S_0 \rightarrow T_3$)	0.53	2.02	0.38	9.71
2.497	LE ($S_0 \rightarrow S_1$)	-1.35	0.90	0.70	4.30
2.586	CT ($S_0 \rightarrow T_4$)	0.54	2.61	0.63	12.55
2.667	CT ($S_0 \rightarrow S_2$)	0.73	2.24	0.35	10.77
3.149	LE ($S_0 \rightarrow T_5$)	-0.91	0.90	0.77	4.34
3.310	LE ($S_0 \rightarrow T_6$)	-1.50	0.53	0.48	2.54
3.315	LE ($S_0 \rightarrow T_7$)	-3.16	0.62	0.86	2.54
3.316	LE ($S_0 \rightarrow S_3$)	-2.52	0.62	0.73	2.97
Dielectric constant = 13.4					
1.609	LE ($S_0 \rightarrow T_1$)	-1.64	0.64	0.71	3.09
2.379	LE ($S_0 \rightarrow T_2$)	-1.32	0.28	0.82	1.32
2.514	LE ($S_0 \rightarrow S_1$)	-1.11	0.80	0.68	3.83
2.515	CT ($S_0 \rightarrow T_3$)	0.55	2.66	0.63	12.79
2.575	CT ($S_0 \rightarrow T_4$)	0.51	2.02	0.38	9.71
2.748	CT ($S_0 \rightarrow S_2$)	0.73	2.24	0.35	10.77
3.206	LE ($S_0 \rightarrow T_5$)	-1.37	0.74	0.78	3.53
3.310	LE ($S_0 \rightarrow T_6$)	-3.28	0.57	0.85	2.75
3.321	LE ($S_0 \rightarrow S_3$)	-2.54	0.77	0.73	3.67
3.339	LE ($S_0 \rightarrow T_7$)	-1.08	0.65	0.48	3.10

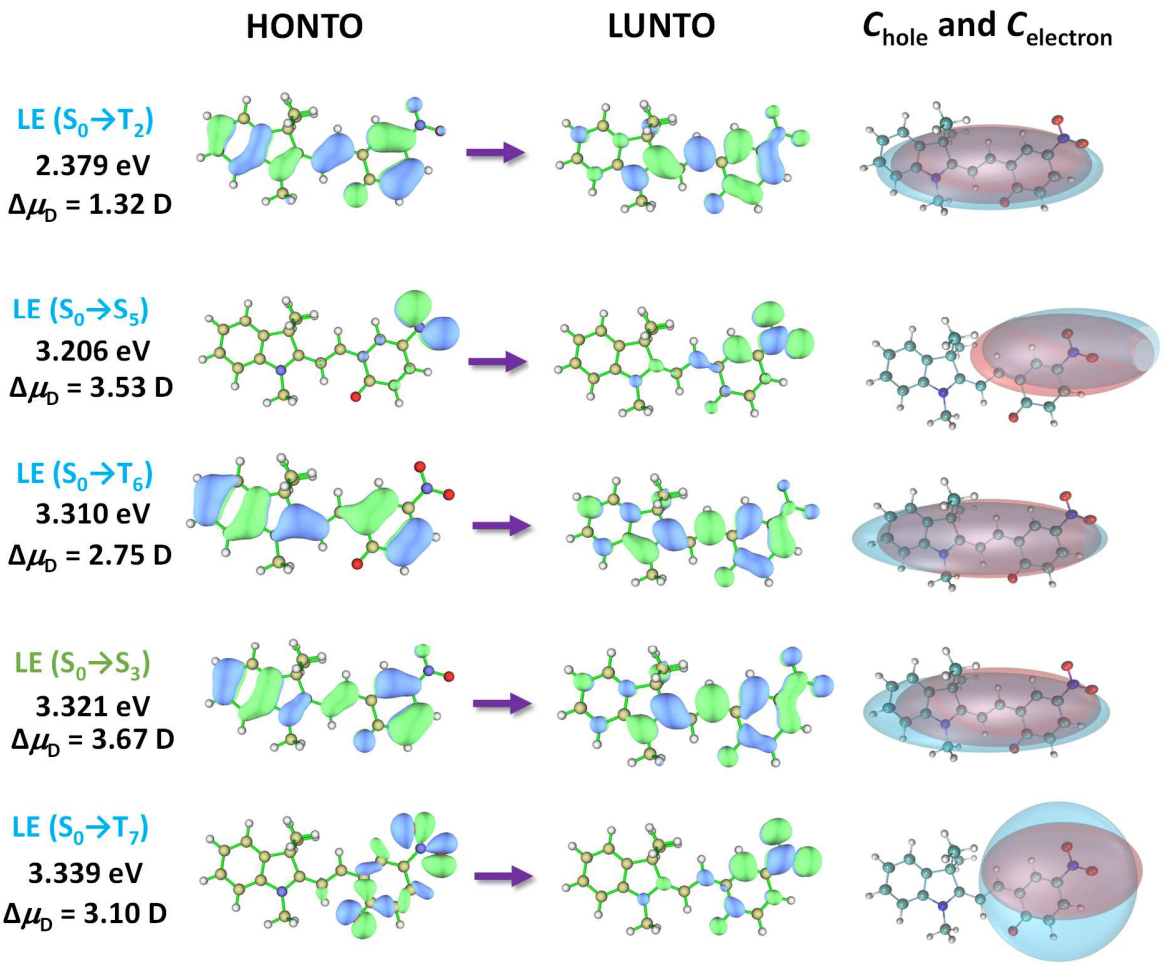

Fig. S9 HONTO, LUNTO and C_{hole} (cyan)/$C_{electron}$ (red) maps of the selected excitations of the MC form. The calculated excitation energy and $\triangle\mu_D$ are indicated.

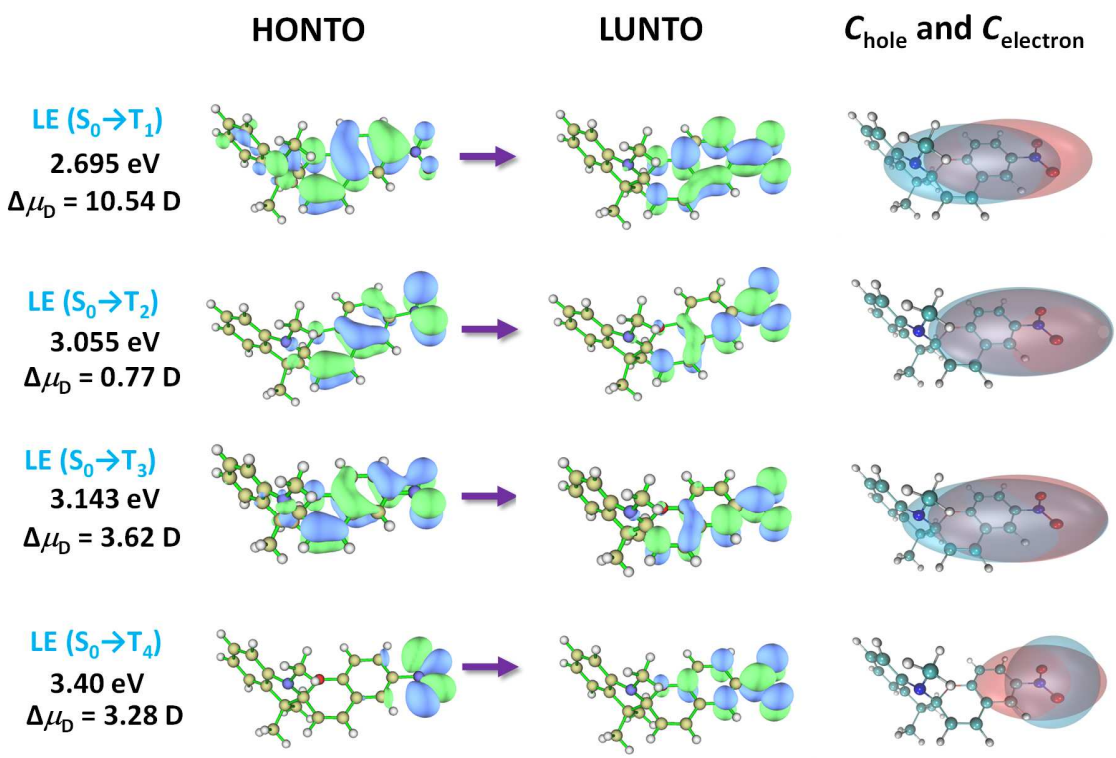

Fig. S10 HONTO, LUNTO and C_{hole} (cyan)/$C_{electron}$ (red) maps of the selected excitations of the SP form. The calculated excitation energy and $\triangle\mu_D$ are indicated.

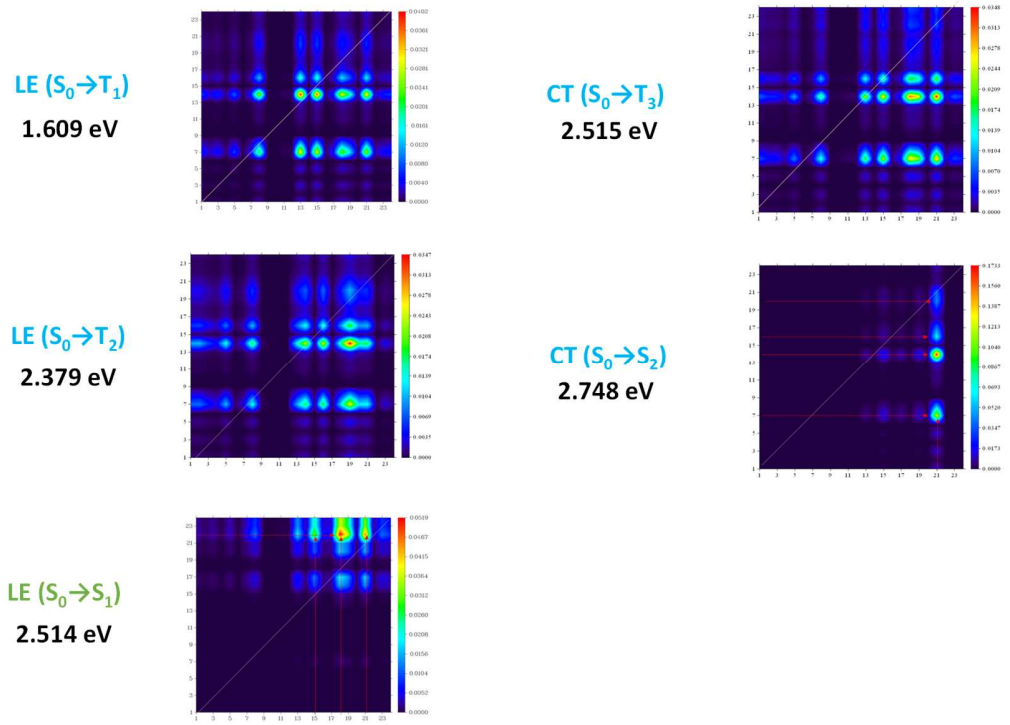

Fig. S11 CTM heat maps of selected CT excitations of the MC molecule.

8. Photoresponse electrical characteristics of the PVP:SP – MC blend – based OPTs with O_2 plasma post–treatment

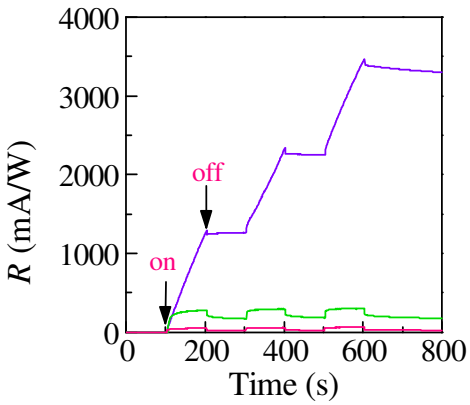

Fig. S12 Real–time photoresponsivity (R) under programmed UV light and visible (green and red) light irradiation of the O_2 plasma post–treated PVP:SP–MC (3:5) blend–based OPTs operated in the saturation regime (V_G = V_D = −2 V). During light irradiation, the "light–on" and "light–off" states were both maintained for 100 s.

References

[s1] D. Li and J. Brisson, *Macromolecules*, 1996, **29**, 868–874.
[s2] J. Dong and Y. Ozaki, *Macromolecules*, 1997, **30**, 286–292.
[s3] X. Luo, S. H. Goh and S. Y. Lee, *Macromolecules*, 1997, **30**, 4934–4938.
[s4] D. J. T. Hill, A. K. Whittaker and K. W. Wong, *Macromolecules*, 1999, **32**, 5285–5291.
[s5] H. Bourara, S. Hadjout, Z. Benabdelghani and A. Etxeberria, *Polymers*, 2014, **6**, 2752–2763.
[s6] P. C. M. F. Castilho, M. R. Crampton and J. Yarwood, *Vib. Spectrosc.*, 1992, **3**, 167–180.
[s7] W. F. Baitinger, P. von R. Schleyer, T. S. S. R. Murty and L. Robinson, *Tetrahedron*, 1964, **20**, 1635–1647.
[s8] Y. Ling, W. C. Xie, G. K. Liu, R. W. Yan, D. Y. Wu and J. Tang, *Sci. Rep.*, 2016, **6**, 31981.
[s9] S. Y. Liu, C. M. Chan, L. T. Weng, L. Li and M. Jiang, M., *Macromolecules*, 2002, **35**, 5623–5629.
[s10] X, Zhou, S. H. Goh, S. Y. Lee and K. L. Tan, *Appl. Surf. Sci.*, 1997, **119**, 60–66.
[s11] K. Roodenko, M. Gensch, J. Rappich, K. Hinrichs, N. Esser and R. Hunger, *J. Phy. Chem. B*, 2007, **111**, 7541–7549.
[s12] M. Chehimi and M. Delamar, *J. Electron. Spectrosc. Relat. Phenom.*, 1987, **43**, 307–314.
[s13] E. Pigois, D. Gayot, M. Delamar, M. Leclerc and M. Chehimi, *J. Electron. Spectrosc. Relat. Phenom.*, 1990, **53**, 79–86.
[s14] M. Chehimi and M. Delamar, *J. Electron. Spectrosc. Relat. Phenom.*, 1988, **46**, 427–434.
[s15] L. Li, C.-M. Chan, L.-T. Weng, M.-L. Xiang and M. Jiang, *Macromolecules*, 1998, **31**, 7248-7255.

[s16] T. Stein, H. Eisenberg, L. Kronik and R. Baer, *Phys. Rev. Lett.,* 2010, **105**, 266802.
[s17] H. L. Cheng, Y. S. Mai, W. Y. Chou, L. R. Chang and X. W. Liang, *Adv. Funct. Mater.*, 2007, **17**, 3639–3649.
[s18] W. Y. Chou, M. H. Chang, H. L. Cheng, Y. C. Lee, C. C. Chang and H. S. Sheu, *J. Phys. Chem. C*, 2012, **116**, 8619–8626.
[s19] L. W. Chung, W. M. C. Sameera, R. Ramozzi, A. J. Page, M. Hatanaka, G. P. Petrova, T. V. Harris, X. Li, Z. Ke, F. Lku, H. B. Li, L. Ding and K. Morokuma, *Chem. Rev.*, 2015, **115**, 5678–5796.